A Non-canonical Reticular-Limbic Central Auditory Pathway via Medial Septum Contributes to Fear Conditioning

Highlights

- A non-canonical, reticular-limbic central auditory pathway was discovered

- It branches from cochlear nucleus and reaches entorhinal cortex via medial septum

- It specifically transmits loud noise-like aversive acoustic signals

- This newly identified pathway contributes to noise-cued fear conditioning

Authors

Guang-Wei Zhang, Wen-Jian Sun, Brian Zingg, ..., Ying Xiong, Huizhong W. Tao, Li I. Zhang

Correspondence

yxiong@tmmu.edu.cn (Y.X.),
htao@usc.edu (H.W.T.),
liizhang@usc.edu (L.I.Z.)

In Brief

Zhang et al. revealed a previously unrecognized central auditory pathway, which is involved in processing aversive acoustic signals and contributes to auditory fear conditioning. It opens a window to reconsider the overall strategy for auditory information processing in the brain.

CellPress

Article

A Non-canonical Reticular-Limbic Central Auditory Pathway via Medial Septum Contributes to Fear Conditioning

Guang-Wei Zhang,[1,2,5] Wen-Jian Sun,[2,3,5] Brian Zingg,[2,4] Li Shen,[2] Jufang He,[3] Ying Xiong,[1,*] Huizhong W. Tao,[2,*] and Li I. Zhang[2,6,*]

[1]Department of Neurobiology, Chongqing Key Laboratory of Neurobiology, Third Military Medical University, 30 Gaotanyan St., Chongqing, 400038, China
[2]Zilkha Neurogenetic Institute, Department of Physiology and Neuroscience, Keck School of Medicine, University of Southern California, Los Angeles, CA 90089, USA
[3]Department of Biology and Chemistry, City University of Hong Kong, Kowloon, Hong Kong
[4]Neuroscience Graduate Program, University of Southern California, Los Angeles, CA 90089, USA
[5]These authors contributed equally
[6]Lead Contact
*Correspondence: yxiong@tmmu.edu.cn (Y.X.), htao@usc.edu (H.W.T.), liizhang@usc.edu (L.I.Z.)
https://doi.org/10.1016/j.neuron.2017.12.010

SUMMARY

In the mammalian brain, auditory information is known to be processed along a central ascending pathway leading to auditory cortex (AC). Whether there exist any major pathways beyond this canonical auditory neuraxis remains unclear. In awake mice, we found that auditory responses in entorhinal cortex (EC) cannot be explained by a previously proposed relay from AC based on response properties. By combining anatomical tracing and optogenetic/pharmacological manipulations, we discovered that EC received auditory input primarily from the medial septum (MS), rather than AC. A previously uncharacterized auditory pathway was then revealed: it branched from the cochlear nucleus, and via caudal pontine reticular nucleus, pontine central gray, and MS, reached EC. Neurons along this non-canonical auditory pathway responded selectively to high-intensity broadband noise, but not pure tones. Disruption of the pathway resulted in an impairment of specifically noise-cued fear conditioning. This reticular-limbic pathway may thus function in processing aversive acoustic signals.

INTRODUCTION

The central auditory system in mammalian brains is a complex system consisting of a number of different nuclei. It starts from the cochlear nucleus (CN), runs through the superior olivary complex (SOC), nucleus of lateral lemniscus (NLL), inferior colliculus (IC), medial geniculate body (MGB) of thalamus, and ends in the auditory cortex (AC) (Webster et al., 1992; Ehret and Romand, 1997). Auditory information is hierarchically relayed along this neuraxis, with distinct auditory features gradually extracted by its component nuclei (Chechik et al., 2006; Escabí and Read, 2003; Webster et al., 1992; Yao et al., 2015; Zhang et al., 2011). There are two parallel ascending pathways along this canonical auditory neuraxis: the lemniscal (primary) and non-lemniscal (secondary) pathways (Hu et al., 1994; Jones, 2003). The primary pathway carries auditory-specific input and peripheral tonotopic maps, while the secondary pathway may be part of an integrative system involved in polysensory integration, temporal pattern recognition, and certain forms of learning (Winer, 1992). Auditory responses in other brain regions are in general attributed to relays from this neuraxis. For example, MGB and AC can provide auditory input to the basolateral amygdala (LeDoux et al., 1985, 1990). Potential major central pathways beyond the canonical auditory neuraxis, however, remain poorly studied.

Besides sensory cortices, the entorhinal cortex (EC) is one of the upper-end structures receiving sensory information. As the main interface between the neocortex and hippocampus, EC functions as a hub in a widespread network for memory and navigation (Buzsáki and Moser, 2013). It is thought that multimodal information from various brain areas, both spatial and non-spatial, is primarily conveyed by EC into the hippocampus (Ahmed and Mehta, 2009; Buzsáki and Moser, 2013; Fyhn et al., 2004; van Strien et al., 2009). Auditory-evoked spiking activity has been reported in EC (Aronov et al., 2017; Rummell et al., 2016; Vinogradov, 1975). Auditory stimuli also increase the c-*fos* staining in EC (Wan et al., 2001). It has been postulated that the auditory input to EC comes from AC or cortical association areas (Moxon et al., 1999), but this idea has rarely been carefully examined in anatomical or functional assays. Since EC also receives potential synaptic projections from a variety of other brain regions that exhibit responses to auditory stimulation, such as the amygdala, septal nuclei, and hippocampal formation (Frank et al., 2000; Justus et al., 2017; Pitkänen et al., 2000), any of these structures might be able to drive auditory responses in EC.

Identifying the neural pathway for relaying auditory information to EC will be crucial for understanding the processing of sensory
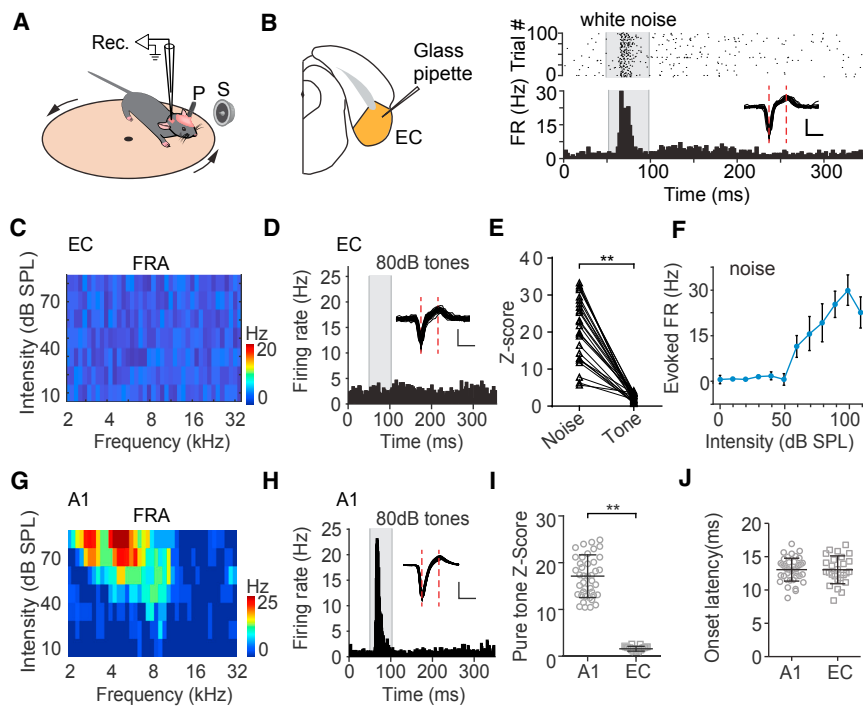
Figure 1. Auditory Responses in EC and A1

(A) Recording setup. P, post for head-fixation; S, speaker. Arrows indicate rotation of the plate.

(B) Left: diagram showing loose-patch recording in EC. Right: spike responses of an example EC neuron to white noise (80 dB SPL). Top: raster plot. Bottom: peri-stimulus spike time histogram (PSTH). Gray box marks the duration of sound stimulation. Inset: superimposed 50 randomly selected spike waveforms. Scale: 50 pA, 0.5 ms.

(C) Color-coded spike rates in response to tones of different frequencies and intensities (i.e., frequency response area) for the same cell.

(D) PSTH generated from spike responses to all test tones at 80 dB SPL for the same cell. Inset, superimposed spike waveforms. Scale: 50 pA, 0.5 ms.

(E) Comparison of Z scores for noise responses (at 80 dB SPL) and tone responses (maximum response within the binned FRA with a 0.5-octave bin size). Data points for the same cell are connected with a line. **$p < 0.01$, paired t test, n = 26 from 5 animals.

(F) Spike rates evoked by noise at different intensity levels (i.e., rate-intensity function) averaged for all the responsive cells (n = 26). Bar represents SD.

(G) Frequency response area of an example A1 neuron.

(H) PSTH generated from spike responses to all test tones at 80 dB SPL for the same A1 neuron.

(I) Comparison of maximum Z scores of pure-tone responses between EC and A1 (n = 41 from 8 animals) neurons. **$p < 0.01$, unpaired two-tailed t test (equal variances not assumed). Bar represents mean ± SD.

(J) Comparison of onset latencies of maximally evoked noise responses between EC and A1 neurons. $p = 0.959$, unpaired two-tailed t test. Bar represents mean ± SD.

cues mediated by this structure. In this study, by combining electrophysiological assays of neuronal response properties, anatomical and functional tracing, as well as optogenetic and pharmacological manipulations, we have elucidated a previously uncharacterized reticular-limbic pathway that diverges from the canonical central auditory pathway at the stage of CN. This identified pathway relays specifically information of high-intensity broadband noise rapidly to EC and thus may be involved in transmitting behaviorally significant aversive auditory signals for emotional and memory functions.

RESULTS

Auditory Responses in the Entorhinal Cortex

To examine auditory responses in EC, we carried out single-cell loose-patch recordings in awake head-fixed mice (see STAR Methods). The animal was free to run on a smoothly rotatable plate (Figure 1A). Auditory stimuli were delivered through a speaker in the contralateral field. As shown by an example EC neuron (Figure 1B), the cell exhibited strong spike responses to white noise at a high intensity of 80 dB sound pressure level (SPL), with an onset latency of 13.2 ms. On the other hand, no clear responses to pure tones were observed, as manifested by the absence of a clear frequency response area (FRA) (Figure 1C) or increased firing rate in the peri-stimulus spike time histogram (PSTH) generated from the responses to test tones (Figure 1D and Figure S1). Noise-evoked spike responses

were observed in about 21% (26 out of 126 recorded neurons, from 11 mice) of the total recorded EC neurons. A similar trend was observed in these auditory responsive EC neurons: they responded robustly to loud noise, but not tones (Figure 1E and Figure S1). As shown by the average rate-intensity function (Figure 1F), these neurons started to respond to noise at around 60 dB SPL, indicating a high intensity threshold. Our recordings were made in both the lateral and medial entorhinal cortex (ECl and ECm, respectively) (Figures S2A and S2B). Neurons in ECl and ECm exhibited similar response properties (Figures S2C–S2E), and they were thus pooled. EC neurons were different from cells in the primary auditory cortex (A1), which exhibited typical V-shaped FRAs and robust tone-evoked responses (Figures 1G–1I). A1 neurons also displayed noise-evoked responses, with onset latencies not different from EC responses (Figure 1J). This comparison of EC and A1 response properties, in particular, the response latency, cast doubt on whether AC or its downstream association areas could be a direct input source for the auditory responses observed in EC.

MS Provides Major Auditory Input to EC

To address the above question, we injected rabies virus encoding GFP into ECl (Figure 2A$_1$). Dense retrogradely labeled cells were observed locally in the EC (Figure 2A$_1$). However, only very sparse neurons were labeled in AC, temporal association area (TEA), and ectorhinal cortex (Figure S3A), and no labeled neurons were found in the auditory thalamus, MGB (Figure S3A).
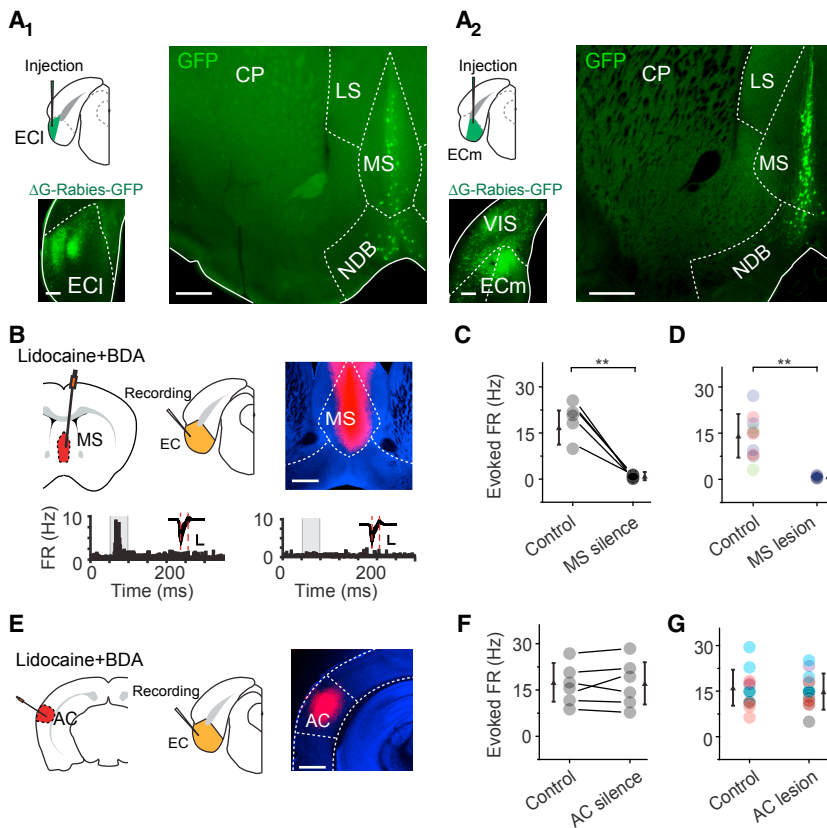
Figure 2. MS Provides Primary Auditory Input to EC

(A₁ and A₂) Injection of rabies virus encoding GFP in the ECl (A₁) or ECm (A₂). Image on the bottom left shows the retrogradely labeled cells around the injection site. Image on the right shows labeled cells in the MS complex. LS, lateral septum; CP, caudoputamen. Scale bar: 500 μm.

(B) Application of lidocaine and BDA (red) into MS and recording from EC. Image on the top right shows representative BDA fluorescence. Scale bar: 500 μm. Bottom: PSTH for responses of an example EC neuron to noise (80 dB SPL) before (left) and after (right) lidocaine application into MS. Insets: superimposed spike waveforms. Scale: 50 pA, 0.5 ms.

(C) Multi-unit spike rates in EC evoked by noise in the control condition and after silencing MS with lidocaine. Data points for the same animal are connected with a line. **p < 0.01, paired t test, n = 5 animals.

(D) Multi-unit spike rates in EC evoked by noise in the control condition and after electrolytic lesion of MS. **p < 0.01, unpaired two-tailed t test, n = 15 sites from 5 animals. Recording sites in the same animal are marked in the same color.

(E) Application of lidocaine and BDA into the auditory cortex and an example image of BDA fluorescence (right). Scale bar: 800 μm.

(F) Multi-unit spike rates in EC evoked by noise in the control condition and after silencing AC with lidocaine. p = 0.823, paired t test, n = 6 animals.

(G) Multi-unit spike rates in EC evoked by noise in the control condition and after electrolytic lesion of AC. p = 0.771, unpaired two-tailed t test, n = 15 sites from 4 animals. Recording sites in the same animal are marked in the same color.

These observations argue against streaming of auditory information mainly from the canonical central pathway to EC. On the other hand, retrogradely labeled cells were robustly found in the medial septum (MS) complex in the basal forebrain, including MS and the central sector of the nucleus of the diagonal band of Broca (NDB) (Figure 2A₁, right), as well as in the hippocampus, retrosplenial cortex (RSP), and claustrum (CLA) (Figures S3B and S3C). These results are in general consistent with recent studies on the mesoscopic connectome of the mouse brain (Oh et al., 2014; Zingg et al., 2014; and data from the Allen Brain Atlas, Experiment 530000865, http://connectivity.brain-map.org/). Rabies viral injections targeted to ECm resulted in similarly dense labeling in the MS complex (Figure 2A₂). Previously, auditory responses have been reported in MS (Vinogradov, 1975), raising the possibility that MS could be a direct input source of EC.

To test whether MS relays auditory information to EC, we perfused lidocaine, a voltage-gated sodium channel blocker, into MS via an implanted cannula (see STAR Methods), while performing extracellular recording in EC (Figure 2B). The drug application site was confirmed by the fluorescence of co-applied biotinylated dextran amine (BDA) (Figure 2B, top right). We found that noise-evoked spike responses of EC neurons were eliminated (Figure 2B, bottom, and Figure 2C) after silencing the MS with lidocaine (Figure S4A). Responses in A1, in contrast, were not affected by silencing MS (Figure S4B). Similarly,

electrolytic lesion of MS (Figure S4D) also blocked auditory responses in EC (Figure 2D and Figure S4D). In contrast, silencing AC with lidocaine (Figure 2E and Figure S4C) or electrolytic lesion of AC (Figure S4E) did not affect auditory responses in EC (Figures 2F and 2G and Figure S4E). Thus, different from a previous postulation (Moxon et al., 1999), we demonstrate that MS rather than AC primarily drives the auditory responses (at least the early responses) observed in EC.

MS Input to EC via Glutamatergic Projections

MS contains neurons of several cell types, including GABAergic, cholinergic, and glutamatergic (Justus et al., 2017; Saunders et al., 2015; Xu et al., 2015). GABAergic MS neurons have been shown to innervate interneurons primarily in EC, and this projection has been thought to mediate a disinhibitory effect in EC (Fuchs et al., 2016; Gonzalez-Sulser et al., 2014; Justus et al., 2017). Glutamatergic neurons have recently been shown to account for about 25% of the MS neuron population (Colom et al., 2005; Robinson et al., 2016). We reasoned that to drive time-locked, sensory-evoked spike rate increases, glutamatergic projections might be more effective than disinhibition mediated by GABAergic projections. To test this possibility, we perfused 6,7-dinitroquinoxaline-2,3-dione (DNQX), a blocker of glutamate receptors, into EC via an implanted cannula, which nearly completely blocked the noise-induced spike rate increases of EC neurons (Figures 3A and 3B), in addition to
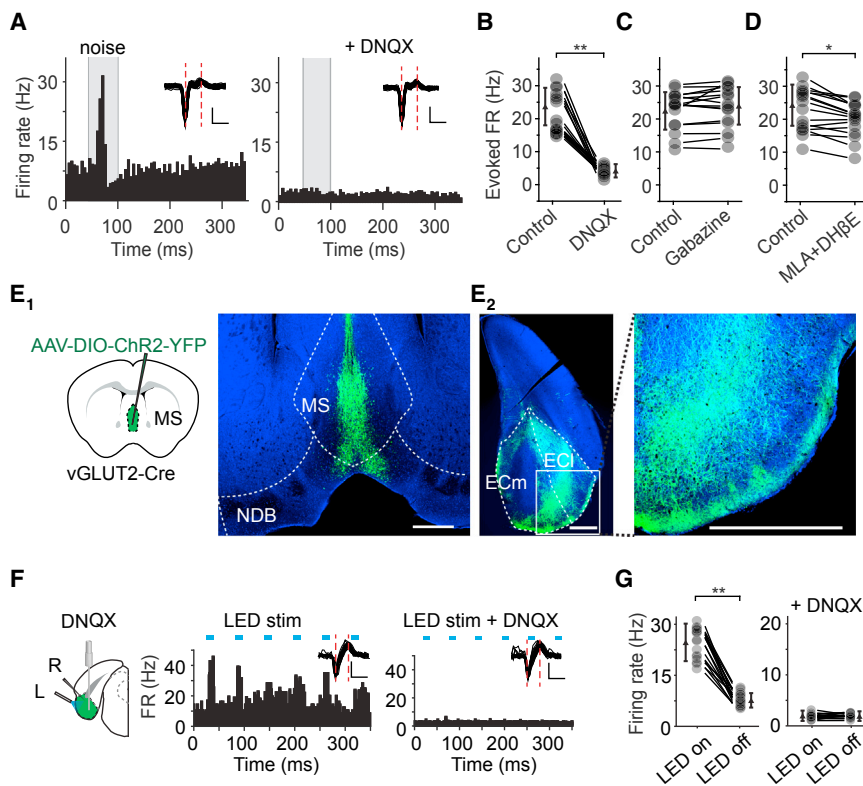
Figure 3. MS Provides Auditory Input to EC via Glutamatergic Projections

(A) PSTH for spike responses of an example EC neuron to noise (80 dB SPL) in the control condition (left) and after perfusing DNQX into EC (right). Scale: 50 pA, 0.5 ms.

(B) Evoked firing rates of EC neurons in the control condition and after DNQX application. **p < 0.01, paired t test, n = 18. Smaller symbols represent mean ± SD.

(C) Evoked firing rates of EC neurons in the control condition and after Gabazine application. p = 0.142, paired t test, n = 17.

(D) Evoked firing rates of EC neurons in the control condition and after MLA and DHβE application. *p < 0.05, paired t test, n = 17.

(E$_1$ and E$_2$) Injection of AAV encoding Cre-dependent ChR2-EYFP into the MS of vGLUT2-Cre mice. Images show fluorescence labeling in the MS complex (E$_1$) and fluorescence-labeled axons in EC (E$_2$, coronal section, an enlarged image of the boxed area is shown on the right). Scale bar: 500 μm.

(F) Application of blue LED light to the EC surface and perfusion of DNQX into EC via a cannula (left). L, LED; R, recording. Middle and right: PSTH for an example EC neuron before and after DNQX application. Blue bars indicate LED pulses. Inset: superimposed spike waveforms. Scale: 50 μV, 0.5 ms.

(G) Spike rates in the presence and absence of LED stimulation in the control condition (left, **p < 0.01, paired t test, n = 18) and after DNQX application (right, p = 0.752, paired t test, n = 15). Spike rate was measured over the time window that starts from the onset of each LED pulse and ends at 10 ms after the offset of the LED pulse.

decreasing the spontaneous firing rate (Figure 3A). In contrast, perfusion of Gabazine, a GABAergic receptor blocker, did not significantly affect the peak evoked firing rate within a 50-ms window immediately after the noise onset (Figure 3C), although late responses might be altered (Figure S5A). Methyllycaconitine (MLA) and dihydro-β-erythroidine (DHβE), which blocked cholinergic receptors (Arroyo et al., 2012), only slightly reduced the response amplitude (Figure 3D and Figure S5B). These data suggest that the auditory responses in EC are mediated primarily by glutamatergic transmission.

We further examined axonal projections of glutamatergic MS neurons by injecting adeno-associated virus (AAV) encoding Cre-dependent channelrhodopsin2 (ChR2) fused with EYFP in vGLUT2-Cre mice (Figure 3E$_1$). Tracing of fluorescence-labeled axons revealed that glutamatergic MS neurons projected strongly to EC (Figure 3E$_2$). We then activated the ChR2-expressing axons by delivering blue LED light (473 nm) onto the surface of EC and recorded spikes from EC neurons (Figure 3F, left). Pulses of LED light could reliably induce phase-locked increases of firing rate (Figure 3F, middle), indicating that the glutamatergic projections from MS can efficiently drive EC cells. In the same cell, perfusion of DNQX into EC completely blocked the LED-evoked spike responses (Figure 3F, right), confirming that glutamatergic transmission mediated these responses. In a total of 17 recorded EC cells (from 3 animals), we observed spike rate increases in response to LED stimulation, which disappeared immediately after the DNQX application (Figure 3G). Together, these data demonstrate that glutamatergic MS projections primarily drive auditory responses of EC neurons.

MS Receives Auditory Input from PCG

We next examined auditory responses in MS by single-unit recording (Figure 4A). About 62% of recorded neurons exhibited acoustic responses (n = 31 out of 50 recorded cells, from 5 animals). Interestingly, these MS neurons exhibited transient responses to white noise (Figure 4A), but no apparent responses to tones (Figure 4B), very similar to EC neurons. In addition, the noise-evoked responses in MS also showed a relatively high intensity threshold (Figure 4C). To test whether MS neurons could be activated in a natural environment, we applied a thunderstorm sound at different intensities, which contained epochs of broadband noise (Figure 4D). MS neurons responded robustly to the thunderstorm sound (Figure 4D), and the responses also showed a relatively high intensity threshold (Figure 4E).

We next traced input sources of MS by injecting ΔG-Rabies-GFP (Figure 4F). One structure in which dense retrogradely labeled cell bodies were observed was the pontine central gray (PCG) (Figure 4F, right), while no cell labeling was found in midbrain nuclei such as the IC and superior colliculus (SC)
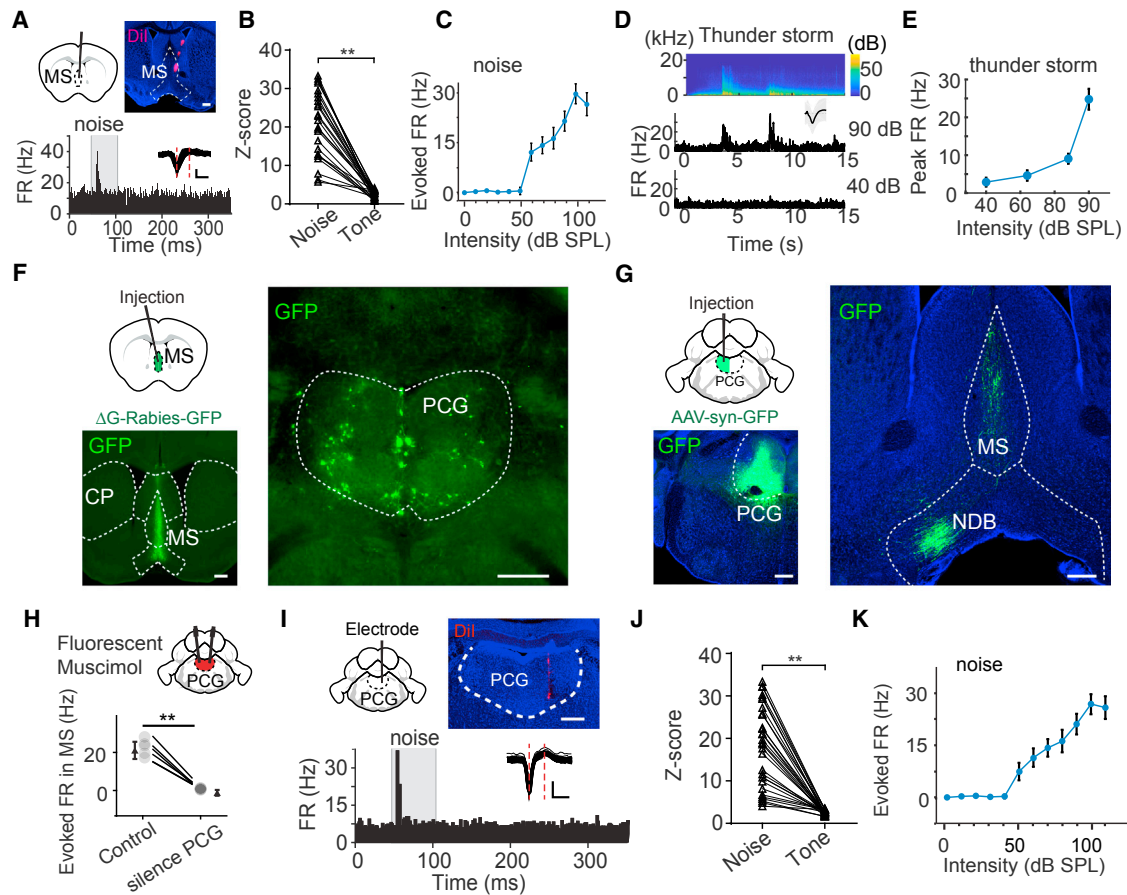
Figure 4. Neurons in MS and Its Input Source PCG Exhibited Similar Response Properties as Those in EC

(A) Recording in MS. Image on top shows the track of recording electrode coated with DiI. Scale bar: 500 μm. Bottom: PSTH for spike responses of an example neuron to white noise (80 dB SPL). Inset: superimposed spike waveforms. Scale: 50 μV, 0.5 ms.

(B) Comparison of Z scores between noise (80 dB SPL) responses and tone responses (maximum within the binned FRA). **p < 0.01, paired t test, n = 31 from 5 animals.

(C) Average rate-intensity function for the responsive MS neurons (n = 31). Bar represents SD.

(D) Top: the spectrogram of thunderstorm sound. Bottom: PSTH for responses of an example MS neuron to thunderstorm sound at two different intensities (90 and 40 dB SPL). Inset, spike waveform.

(E) Average rate-intensity function for MS neurons responding to thunderstorm sound (n = 23).

(F) Injection of ΔG-Rabies-GFP into MS. Images show GFP fluorescence in the MS complex (left) and retrogradely labeled cell bodies in the PCG (right). Scale bar: 500 μm.

(G) Injection of AAV-syn-GFP into PCG. Images show GFP fluorescence in PCG (left) and GFP-labeled axons in the MS complex (right). Scale bar: 500 μm.

(H) Bilateral perfusion of fluorescent muscimol into PCG. Bottom, noise-evoked multi-unit spike rates recorded in MS in the control condition and after silencing PCG with muscimol. **p < 0.01, n = 5 animals, paired t test.

(I) PSTH for responses of an example PCG neuron to noise (80 dB SPL). Image on top shows the track of electrode. Scale: 500 μm. Inset: spike waveforms. Scale: 50 μV, 0.5 ms.

(J) Comparison of Z scores between noise and tone (maximally evoked within the FRA) responses. **p < 0.01, paired t test, n = 30 PCG neurons from 5 animals.

(K) Average rate-intensity function for all the responsive PCG neurons (n = 30 from 5 animals). Bar represents SD.

(data not shown). Anterograde tracing of PCG axons confirmed that they projected to MS (Figure 4G). To test whether PCG provided auditory input to MS, we perfused muscimol into PCG while performing extracellular recording in MS. We found that noise-evoked multi-unit spike responses in the control condition were eliminated by silencing PCG (Figure 4H), confirming that PCG provided auditory input to MS. We further carried out single-unit recording in PCG to characterize its auditory response properties. As shown by an example cell (Figure 4I) and summary

of 30 responsive cells (out of 42 recorded cells, from 5 animals) (Figures 4J and 4K), PCG neurons exhibited response properties similar to MS and EC neurons, i.e., they responded robustly to high-intensity noise but not to tones.

PRN Relays Auditory Information from CN to PCG

We further traced input sources of PCG by injecting AAVretro-Cre into Ai14, a Cre-dependent tdTomato reporter line (Madisen et al., 2010). We found tdTomato-labeled cell bodies in the dorsal part
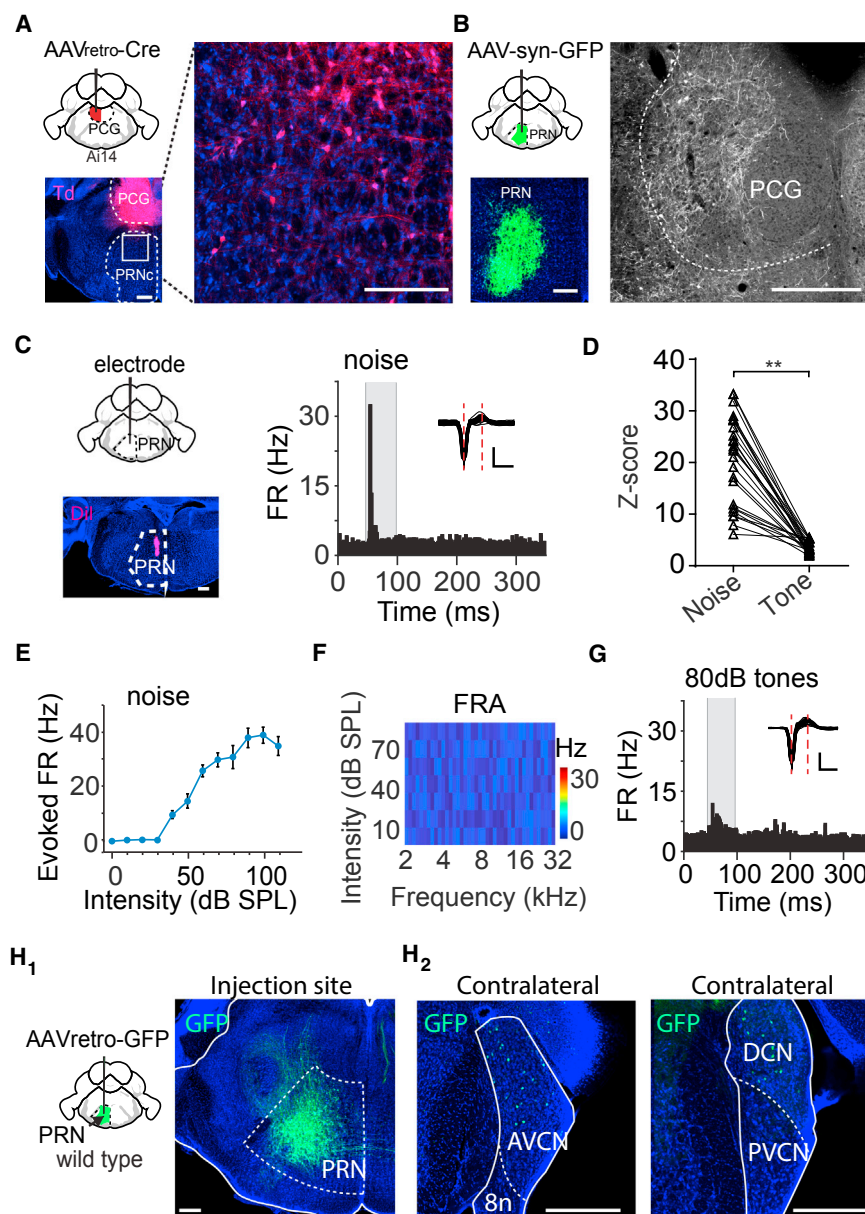
Figure 5. PRN Relays Auditory Information from CN to PCG

(A) Injection of AAVretro-Cre into PCG of Ai14 mice. Images show strong tdTomato labeling in the PCG (left) and labeled cells in the dorsal part of PRNc (right, which is an enlarged image of the boxed area on the left). Scale bar: 500 μm.

(B) Injection of AAV-syn-GFP into PRN. Images show GFP labeling in PRN (left) and labeled axons in PCG (right). Scale bar: 500 μm.

(C) Recording in the PRN region. Image on the left shows the electrode track. Right, PSTH for responses of an example PRN neuron to noise (80 dB SPL). Inset, spike waveforms. Scale: 50 μV, 0.5 ms.

(D) Comparison of Z scores between noise and tone responses. **$p < 0.01$, paired t test, n = 23 from 5 animals.

(E) Average rate-intensity function for PRN neurons (n = 23 from 5 animals). Bar represents SD.

(F) Frequency response area of an example PRN neuron.

(G) PSTH of spike responses of the same cell to test tones at 80 dB SPL.

(H_1 and H_2) Injection of AAVretro-GFP into PRNc. Images show GFP fluorescence around the injection site (H_1, right) and retrogradely labeled cell bodies in the contralateral CN (H_2). Scale bar: 500 μm. AVCN, anterior ventral cochlear nucleus; PVCN, posterior ventral cochlear nucleus; DCN, dorsal cochlear nucleus; 8n, eighth nerve.

ear (Webster et al., 1992). Therefore, PRN can relay auditory information from CN to PCG.

The Reticular-Limbic Ascending Auditory Pathway

The above experiments suggest a non-canonical central auditory pathway from the CN to PRN, to PCG, to MS, and then to EC. We compared response properties between this reticular-limbic pathway and the canonical lemniscal pathway leading to AC. At each successive stage downstream of CN, neurons in the reticular-limbic pathway exhibited significantly higher intensity thresholds than those in the canonical pathway (Figure 6A). The high intensity threshold first emerged in PRN and persisted across the successive stages of the reticular-limbic pathway. The onset latency of auditory responses (quantified for responses to noise at 80 dB SPL) was progressively increased along both pathways (Figure 6B), consistent with a serial connection scheme. The response latency in MS was comparable to that in the auditory thalamus (ventral MGB), while the latency in EC was comparable to that in A1 (Figure 6B). These data indicate that via the relay by the reticular-limbic pathway, EC can receive auditory information as fast as A1.

To further demonstrate the functional separation between the reticular-limbic and canonical central pathways in our

of the caudal pontine reticular nucleus (PRNc) (Figure 5A). Anterograde tracing of PRN axons confirmed their projections to PCG (Figure 5B), but not to MS (Figure S6). Single-unit recordings in the dorsal part of PRNc again demonstrated similar auditory response properties as in PCG, MS, and EC (Figures 5C–5G), except that the intensity threshold was slightly lower (Figure 5E). Finally, by injecting AAVretro-GFP into PRNc (Figure 5H_1), we found that the input to PRNc could be traced back to the contralateral CN, including the anteroventral and dorsal cochlear nucleus (AVCN and DCN, respectively) (Figure 5H_2), consistent with previous reports (Kandler and Herbert, 1991; Lee et al., 1996), as well as the anterograde tracing data of the Allen Brain Atlas (Experiment 286556914, http://connectivity.brain-map.org/). CN is known to receive auditory input directly from the inner
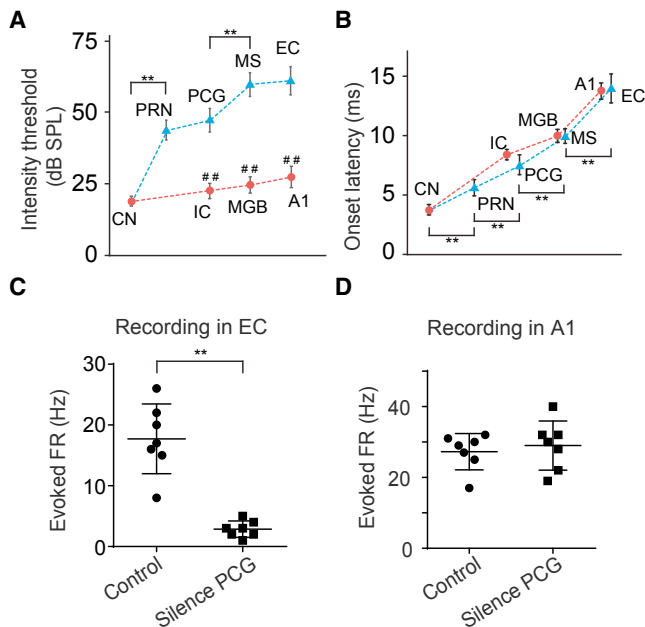
Figure 6. Comparison of Response Properties between Two Central Auditory Pathways

(A) Average intensity thresholds as determined by responses to noise at successive stages of the reticular-limbic (blue) and canonical lemniscal (red) pathways. Bar represents SD. N = 21 for CN (from 5 animals), 23 for IC (from 4 animals), 18 for MGBv (from 5 animals), and 56 for A1 (from 8 animals). **p < 0.01, in comparison with the previous stage in the same pathway, one-way ANOVA post hoc (Tukey) test. ##p < 0.01, in comparison with the corresponding stage in the other pathway, unpaired two-tailed t test.

(B) Average response onset latencies at different stages. Bar represents SD. **p < 0.01, in comparison with the previous stage in the same reticular-limbic pathway, one-way ANOVA post hoc (Tukey) test.

(C) Noise-induced multi-unit responses in EC before and after silencing PCG (n = 7 sites from 3 animals). **p < 0.01, unpaired two-tailed t test. Bar represents mean ± SD.

(D) Noise-induced multi-unit responses in A1 before and after silencing PCG (n = 7 sites from 3 animals). p = 0.48, unpaired two-tailed t test.

experimental condition, we performed multi-unit recording in EC or A1 and silenced PCG with muscimol. Silencing PCG blocked noised-evoked spike responses in EC (Figure 6C) but did not affect auditory responses in A1 (Figure 6D).

Involvement in Auditory-Related Conditioned Fear Memory

It has been well documented that PRNc mediates acoustic startle response (ASR) (Koch and Schnitzler, 1997; Lee et al., 1996). We first examined whether the identified reticular-limbic pathway could play a role in ASR by monitoring the Preyer's reflex, manifested by movements of pinna immediately following the exposure to a loud sound (Jero et al., 2001) (Figure 7A). In the control condition, noise (80 dB SPL) successfully elicited the Preyer's reflex in >90% of randomly tested trials, and tones (80 dB SPL, 7.5 kHz) induced weaker reflexive responses in a slightly lower percentage of trials (Figure 7B). Neither silencing PCG with muscimol nor silencing MS with lidocaine had any

effect on the reflexive response (Figure 7B), indicating that the reticular-limbic pathway is not involved in ASR.

EC is known to be involved in memory functions (Andersen et al., 2006; Buzsáki and Moser, 2013; Li et al., 2017). We wondered whether the reticular-limbic pathway to EC could play a role in establishing auditory-related memory. To test this possibility, we employed a classic conditioned fear response assay (Fanselow and Poulos, 2005; Letzkus et al., 2011; Romanski and LeDoux, 1992). For conditioning, mice were exposed to five pairings of a conditioned stimulus (CS, 20 s white noise, 80 dB SPL) and a foot shock (unconditioned stimulus [US]) (Figure 7C). On the following day, they were exposed to the CS alone without foot shocks in a different context as to measure the cued conditioned response (Figure 7C), which was quantified as the percentage of time freezing during the presentation of CS. Naive animals having not experienced the pairings of CS and US did not exhibit freezing upon CS presentation, whereas conditioned control and saline-perfused control (EC-perfused, 85% ± 4%, n = 5; MS-perfused, 89% ± 7%, n = 4; PCG-perfused, 87% ± 5%, n = 4) animals exhibited robust freezing on the testing day (Figure 7D). Perfusion of lidocaine into EC bilaterally just before parings of CS and US, i.e., to silence EC activity during conditioning, dramatically reduced the freezing time measured on the following day (Figure 7D, ΔEC), consistent with the previous notion of involvement of EC in the formation of fear memory (Baldi et al., 2013; Sparta et al., 2014). Silencing MS or PCG activity during pairings of CS and US also significantly impaired the freezing response, although to a lesser extent (Figure 7D, ΔMS, ΔPCG). In contrast, silencing AC during conditioning had no effect on the freezing response on the testing day (Figure 7D, ΔAC).

Since neurons in the reticular-limbic pathway exhibited little response to tones, we reasoned that tone-conditioned fear memory might not be affected by interrupting this pathway. To test this idea, we trained mice by pairing a tone (80 dB SPL, 7.5 kHz) with a foot shock for ten times. Control mice exhibited robust freezing on the testing day after conditioning (Figure 7E). Silencing MS and PCG during conditioning had no effect on the freezing time (Figure 7E), indicating that the reticular-limbic pathway is not involved in tone-conditioned fear learning. Consistent with a previous study (Romanski and LeDoux, 1992), we found that AC was also not required for tone-cued fear conditioning (Figure 7E). It should be noted that different results have also been reported (e.g., Banerjee et al., 2017), which may be attributed to differences in experimental conditions. As summarized in Figure 7F, disrupting activity in nuclei of the reticular-limbic pathway during conditioning specifically reduced noise- but not tone-conditioned fear response, indicating that this pathway plays a role in transmitting specifically noise signals for the formation of auditory-related conditioned fear memory.

DISCUSSION

Auditory Responses in the Limbic System

Information processing in the mammalian brain relies on a hierarchical relay of sensory input along central processing
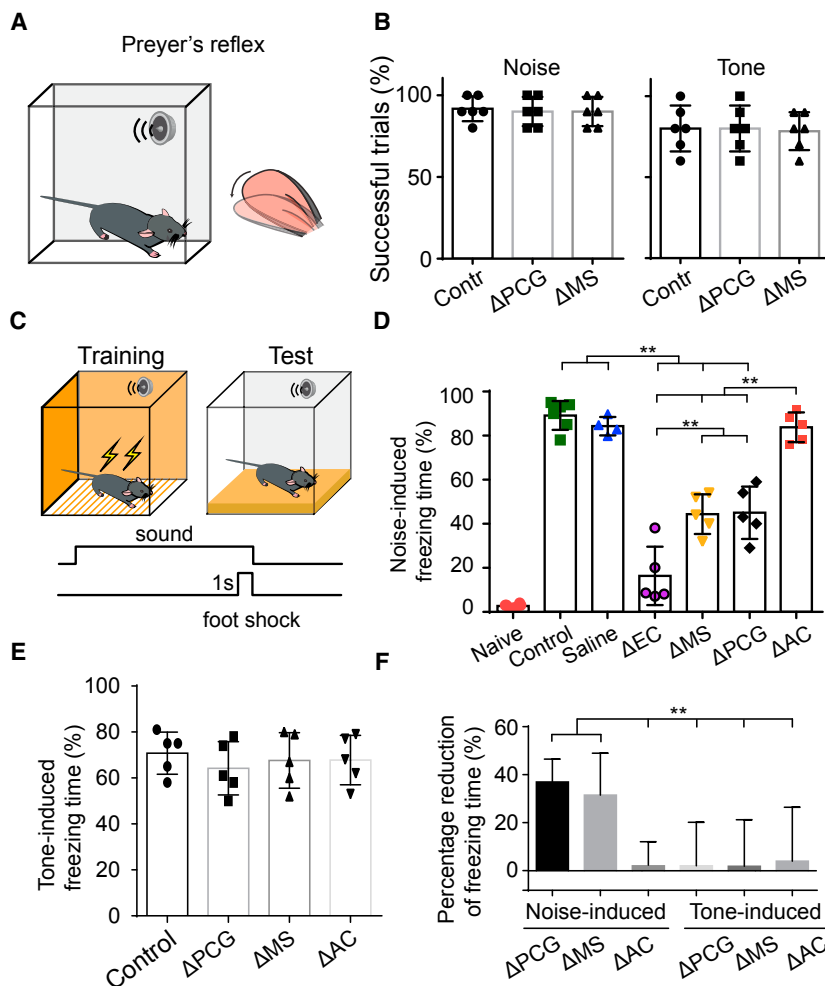
Figure 7. The Reticular-Limbic Pathway Plays a role in Auditory-Related Conditioned Fear Memory

(A) A schematic illustration of test of the Preyer's reflex.

(B) Percentage of successful trials showing Preyer's reflex immediately following noise (left) or tone (right) presentation for the control group (n = 6 animals) as well as PCG (n = 6 animals, bilaterally with muscimol) and MS (n = 6 animals, bilaterally with lidocaine) silencing groups. Each data point represents one animal. Bar represents SD.

(C) Diagram showing the conditioned fear response assay. For training, 1-s foot shock co-terminated with 20-s sound.

(D) Percentage freezing time during presentation of noise (80 dB SPL) alone on the testing day for naive (n = 6 animals), noise-conditioned control (n = 6), saline-injected control (n = 4, into EC) groups as well as for experimental groups in which EC (n = 5, with lidocaine), MS (n = 5, with lidocaine), PCG (n = 5, with muscimol), or AC (n = 5, with lidocaine) was silenced during conditioning. Bar represents SD. **p < 0.01, one-way ANOVA post hoc (Tamhane) test.

(E) Percentage freezing time during presentation of tones (80 dB SPL, 7.5 kHz) alone in the tone-conditioned control (n = 5 animals), as well as in the experimental groups in which MS (n = 5), PCG (n = 5) or AC (n = 5) was silenced during conditioning. Bar represents SD.

(F) Summary of percentage reduction of freezing time in experimental groups in which MS, PCG, or AC was silenced during conditioning [(experimental – saline-injected control)/experimental, bootstrap resampling]. Bar represents mean ± SD. **p < 0.01, unpaired t test.

pathways. To understand this process, it is fundamental to characterize neuronal responses at each stage of these pathways. In the auditory system, previous studies have predominantly focused on the well-characterized auditory neuraxis from the CN to AC. However, in several earlier studies, auditory responses have also been reported in brain regions beyond the canonical neuraxis, in particular, the nuclei associated with the limbic system, e.g., the cingulate cortex, lateral and basolateral amygdala, dentate gyrus of hippocampal formation, septum, entorhinal cortex, and mammillary body (Vinogradov, 1975). In those studies, auditory response properties have not been characterized quantitatively. It thus has remained unclear what auditory pathways are underlying these acoustic responses. In the present study, we compared neuronal responses to noise and tone stimuli and their temporal properties in the limbic system. Our findings of MS and EC neurons responding specifically to high-intensity noise are consistent with previous observations that neurons in the limbic system could be driven more efficiently by loud click sounds (Vinogradov, 1975) and that tone-evoked Ca²⁺ responses were absent at the EC axon terminals in the hippocampus (Lovett-Barron et al., 2014).

Auditory Responses in Pontine Nuclei

PRNc is known to be involved in acoustic startle response (Koch and Schnitzler, 1997; Lee et al., 1996). For this reflexive behavior, PRNc neurons receive auditory input from the cochlear nucleus and project to the spinal cord to drive motor neurons, resulting in muscle contractions (Koch and Schnitzler, 1997). Our behavioral experiments demonstrate that disrupting activity of the nuclei in the reticular-limbic pathway downstream of PRNc does not affect ASR (Figure 7B). Therefore, the pathway delineated in this study is likely separate from the circuit mediating ASR, although it also relies on PRNc to receive auditory input (Figure 8).

It has been observed previously that PRN neurons respond to tone stimuli only with intensity as high as 80 dB SPL (Lee et al., 1996; Lingenhöhl and Friauf, 1994). Our result confirmed this point (Figure 5G). More importantly, our data show that PRN neurons can be more efficiently driven by noise stimuli, with a moderate intensity threshold. This may result from a convergence of multiple relatively weak CN inputs with different frequency preferences onto a single PRN neuron. Consistent with a previous report (Kandler and Herbert, 1991), our retrograde labeling experiments indicate that both AVCN and DCN project
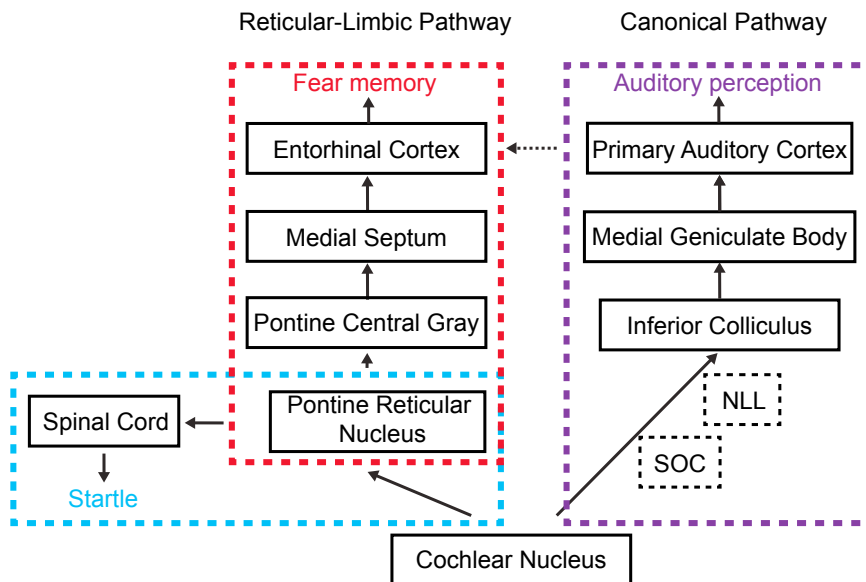
Reticular-Limbic Pathway   Canonical Pathway

Figure 8. Summary of Serial Connections in the Reticular-Limbic and Canonical Lemniscal Pathways
The former diverges from the latter at the stage of CN. The circuit specific for ASR is boxed with blue color. The sparse projections from AC to EC are labeled with a dotted line. NLL, the nucleus of lateral lemniscus; SOC, superior olivary complex.

ously observed in MS (Miller and Freedman, 1993; Vinogradov, 1975), the structure has mostly been implicated in driving oscillatory activity in the hippocampus and relaying information of locomotion speed (Fuhrmann et al., 2015; Justus et al., 2017; Robinson et al., 2016). In the present study, we showed that MS neurons could respond robustly to broadband noise contained in natural sounds. It is thus possible that MS can perform multiple functions, possibly through recruiting distinct types (Gonzalez-Sulser et al., 2014; Saunders et al., 2015) or subsets of neurons under different contexts.

to PRN, suggesting that a variety of CN cell types, e.g., giant neurons in deep layers of DCN (Romand, 1997), may provide input to PRN neurons.

Modulation of PRN activity has been implicated in the prepulse inhibition of ASR (Carlson and Willott, 1998; Lingenhöhl and Friauf, 1994). In this case, PRN is considered as a terminal structure where multiple forms of modulation can take effect (Koch and Schnitzler, 1997). However, the roles of its broad projections to the reticular formation and midbrain (Iwasaki et al., 1999) remain unknown. In this study, our results suggest that PCG integrates auditory information from the PRN and then relays it to the forebrain. Since PRN is multisensory (Yeomans et al., 2002), it is likely that multisensory information can also be relayed via PCG to MS.

A Non-canonical Central Auditory Pathway

Our study, for the first time, has elucidated a complete central relay pathway divergent from the canonical auditory neuraxis (Figure 8). We demonstrate that auditory responses, at least the early responses, in EC are primarily driven by MS. This is supported by both the anatomical and pharmacological evidence. It appears that the reticular-limbic and canonical pathways are mostly independent of each other, since silencing MS has no effect on auditory responses in AC (Figure S4B) and silencing AC has no effect on the responses in EC (Figure 2F). On the other hand, we should note that our anatomical data (Figure S3) and previous tracing results (Allen Brain Atlas, http://connectivity.brain-map.org/) both indicate that there are relatively sparse projections from AC to EC and that EC may also receive indirect inputs from AC via TEA, ectorhinal, or perirhinal cortical regions (Burwell and Amaral, 1998; Kotak et al., 2015). Since in this study we have focused explicitly on short-latency responses in EC, it remains possible that AC-mediated direct or indirect inputs can contribute to some late responses. The functional interactions between AC and EC remain to be further investigated in the future.

It is somewhat surprising to find that MS relays the primary auditory input to EC. Although auditory responses were previ-

Functional Implication for the Reticular-Limbic Auditory Pathway

The limbic system, especially its components EC, MS, and hippocampus, is known to be critically involved in memory functions (Andersen et al., 2006). It is thus straightforward to postulate that one functional purpose of the reticular-limbic pathway is to relay some salient signals rapidly for memory storage or retrieval. Neurons in PRN acquire auditory response properties very different from their source neurons in CN, indicating that sound information has been filtered at this stage. Across all the successive stages, broadband noise stimuli more efficiently drive neuronal responses than pure tones, although tones of very high intensity (>90 dB SPL) may elicit some responses (data not shown). In our previous studies, we have shown that loud noise can trigger flight response in rodents (Xiong et al., 2015; Zingg et al., 2017). Thus the pathway delineated in this study appears to specifically convey acoustic information of aversive nature. As EC projects to the dentate gyrus of the hippocampus and primarily drives auditory responses there (Deadwyler et al., 1981), the reticular-limbic pathway may provide a route for the fast relay of aversive, behaviorally significant acoustic signals to the hippocampus.

It is interesting to note that silencing EC produced a larger effect on fear conditioning than disrupting each earlier stage in the reticular-limbic pathway (Figure 7D). We reason that EC is likely a late-stage center for integrating information from various sources essential for the formation of fear memory. That is, it receives input not only from MS as we demonstrate in this study, but also from other pathways, e.g., via the amygdala, which is also important for the formation of fear memory (LeDoux, 2012). In addition, our data demonstrate that inactivating each stage of the reticular-limbic pathway

during conditioning impairs noise-conditioned but not tone-conditioned fear memory. This result is consistent with the observation that this pathway transmits little tone information and suggests that transmitting noise signals along the pathway is essential for the formation of noise-specific conditioned fear memory. On the other hand, tone signals may be transmitted through other pathways, e.g., via the amygdala (Ehrlich et al., 2009; Haubensak et al., 2010; Wolff et al., 2014), to form tone-specific fear memory. How the auditory information of noise is processed beyond EC will be of great interest for future investigations.

STAR★METHODS

Detailed methods are provided in the online version of this paper and include the following:

- KEY RESOURCES TABLE
- CONTACT FOR REAGENT AND RESOURCE SHARING
- EXPERIMENTAL MODELS AND SUBJECT DETAILS
- METHOD DETAILS
  - Head-fixed animal preparation
  - *In vivo* electrophysiological recordings in awake animals
  - Sound stimulation
  - Viral injection
  - Optogenetic activation
  - Silencing of brain structures
  - Fear conditioning
  - Test of the Preyer's reflex
- QUANTIFICATION AND STATISTICAL ANALYSIS
  - Data processing
  - Statistics

SUPPLEMENTAL INFORMATION

Supplemental Information includes six figures and can be found with this article online at https://doi.org/10.1016/j.neuron.2017.12.010.

AUTHOR CONTRIBUTIONS

L.I.Z. and H.W.T. conceived the study. G.-W.Z. performed most behavioral and recording experiments. W.-J.S. started and contributed to early behavioral and recording experiments. B.Z. contributed to anatomical experiments. L.S. contributed to recordings and data analysis. J.H. contributed to discussion. L.I.Z., H.W.T., and Y.X. supervised the project. L.I.Z., H.W.T., and G.W.Z. wrote the manuscript.

DECLARATION OF INTERESTS

The authors declare no competing interests.

REFERENCES

Ahmed, O.J., and Mehta, M.R. (2009). The hippocampal rate code: anatomy, physiology and theory. Trends Neurosci. *32*, 329–338.

Andersen, P., Morris, R., Amaral, D., Bliss, T., and O'Keefe, J. (2006). The Hippocampus Book (Oxford University Press).

Aronov, D., Nevers, R., and Tank, D.W. (2017). Mapping of a non-spatial dimension by the hippocampal-entorhinal circuit. Nature *543*, 719–722.

Arroyo, S., Bennett, C., Aziz, D., Brown, S.P., and Hestrin, S. (2012). Prolonged disynaptic inhibition in the cortex mediated by slow, non-α7 nicotinic excitation of a specific subset of cortical interneurons. J. Neurosci. *32*, 3859–3864.

Baldi, E., Liuzzo, A., and Bucherelli, C. (2013). Fimbria-fornix and entorhinal cortex differential contribution to contextual and cued fear conditioning consolidation in rats. Physiol. Behav. *114-115*, 42–48.

Banerjee, S.B., Gutzeit, V.A., Baman, J., Aoued, H.S., Doshi, N.K., Liu, R.C., and Ressler, K.J. (2017). Perineuronal nets in the adult sensory cortex are necessary for fear learning. Neuron *95*, 169–179.e3.

Burwell, R.D., and Amaral, D.G. (1998). Perirhinal and postrhinal cortices of the rat: interconnectivity and connections with the entorhinal cortex. J. Comp. Neurol. *391*, 293–321.

Buzsáki, G., and Moser, E.I. (2013). Memory, navigation and theta rhythm in the hippocampal-entorhinal system. Nat. Neurosci. *16*, 130–138.

Carlson, S., and Willott, J.F. (1998). Caudal pontine reticular formation of C57BL/6J mice: responses to startle stimuli, inhibition by tones, and plasticity. J. Neurophysiol. *79*, 2603–2614.

Chechik, G., Anderson, M.J., Bar-Yosef, O., Young, E.D., Tishby, N., and Nelken, I. (2006). Reduction of information redundancy in the ascending auditory pathway. Neuron *51*, 359–368.

Colom, L.V., Castaneda, M.T., Reyna, T., Hernandez, S., and Garrido-Sanabria, E. (2005). Characterization of medial septal glutamatergic neurons and their projection to the hippocampus. Synapse *58*, 151–164.

Deadwyler, S.A., West, M.O., and Robinson, J.H. (1981). Entorhinal and septal inputs differentially control sensory-evoked responses in the rat dentate gyrus. Science *211*, 1181–1183.

Dong, H. (2007). The Allen Reference Atlas: A Digital Color Brain Atlas of the C57BL/6J Male Mouse (John Wiley and Sons).

Ehret, G., and Romand, R. (1997). The Central Auditory System (Oxford University Press).

Ehrlich, I., Humeau, Y., Grenier, F., Ciocchi, S., Herry, C., and Lüthi, A. (2009). Amygdala inhibitory circuits and the control of fear memory. Neuron *62*, 757–771.

Escabí, M.A., and Read, H.L. (2003). Representation of spectrotemporal sound information in the ascending auditory pathway. Biol. Cybern. *89*, 350–362.

Fanselow, M.S., and Poulos, A.M. (2005). The neuroscience of mammalian associative learning. Annu. Rev. Psychol. *56*, 207–234.

Frank, L.M., Brown, E.N., and Wilson, M. (2000). Trajectory encoding in the hippocampus and entorhinal cortex. Neuron *27*, 169–178.

Fuchs, E.C., Neitz, A., Pinna, R., Melzer, S., Caputi, A., and Monyer, H. (2016). Local and distant input controlling excitation in layer II of the medial entorhinal cortex. Neuron *89*, 194–208.

Fuhrmann, F., Justus, D., Sosulina, L., Kaneko, H., Beutel, T., Friedrichs, D., Schoch, S., Schwarz, M.K., Fuhrmann, M., and Remy, S. (2015). Locomotion, theta oscillations, and the speed-correlated firing of hippocampal neurons are controlled by a medial septal glutamatergic circuit. Neuron *86*, 1253–1264.

Fyhn, M., Molden, S., Witter, M.P., Moser, E.I., and Moser, M.-B. (2004). Spatial representation in the entorhinal cortex. Science *305*, 1258–1264.

Gonzalez-Sulser, A., Parthier, D., Candela, A., McClure, C., Pastoll, H., Garden, D., Sürmeli, G., and Nolan, M.F. (2014). GABAergic projections from the medial septum selectively inhibit interneurons in the medial entorhinal cortex. J. Neurosci. *34*, 16739–16743.

Haubensak, W., Kunwar, P.S., Cai, H., Ciocchi, S., Wall, N.R., Ponnusamy, R., Biag, J., Dong, H.W., Deisseroth, K., Callaway, E.M., et al. (2010). Genetic dissection of an amygdala microcircuit that gates conditioned fear. Nature *468*, 270–276.

Hu, B., Senatorov, V., and Mooney, D. (1994). Lemniscal and non-lemniscal synaptic transmission in rat auditory thalamus. J. Physiol. *479*, 217–231.

Ibrahim, L.A., Mesik, L., Ji, X.Y., Fang, Q., Li, H.F., Li, Y.T., Zingg, B., Zhang, L.I., and Tao, H.W. (2016). Cross-modality sharpening of visual cortical processing through layer-1-mediated inhibition and disinhibition. Neuron *89*, 1031–1045.

Iwasaki, H., Kani, K., and Maeda, T. (1999). Neural connections of the pontine reticular formation, which connects reciprocally with the nucleus prepositus hypoglossi in the rat. Neuroscience *93*, 195–208.

Jero, J., Coling, D.E., and Lalwani, A.K. (2001). The use of Preyer's reflex in evaluation of hearing in mice. Acta Otolaryngol. *121*, 585–589.

Jones, E.G. (2003). Chemically defined parallel pathways in the monkey auditory system. Ann. N Y Acad. Sci. *999*, 218–233.

Justus, D., Dalügge, D., Bothe, S., Fuhrmann, F., Hannes, C., Kaneko, H., Friedrichs, D., Sosulina, L., Schwarz, I., Elliott, D.A., et al. (2017). Glutamatergic synaptic integration of locomotion speed via septoentorhinal projections. Nat. Neurosci. *20*, 16–19.

Kandler, K., and Herbert, H. (1991). Auditory projections from the cochlear nucleus to pontine and mesencephalic reticular nuclei in the rat. Brain Res. *562*, 230–242.

Koch, M., and Schnitzler, H.-U. (1997). The acoustic startle response in rats–circuits mediating evocation, inhibition and potentiation. Behav. Brain Res. *89*, 35–49.

Kotak, V.C., Mowery, T.M., and Sanes, D.H. (2015). Characterization of auditory synaptic inputs to gerbil perirhinal cortex. Front. Neural Circuits *9*, 40.

LeDoux, J. (2012). Rethinking the emotional brain. Neuron *73*, 653–676.

LeDoux, J.E., Ruggiero, D.A., and Reis, D.J. (1985). Projections to the subcortical forebrain from anatomically defined regions of the medial geniculate body in the rat. J. Comp. Neurol. *242*, 182–213.

LeDoux, J.E., Farb, C., and Ruggiero, D.A. (1990). Topographic organization of neurons in the acoustic thalamus that project to the amygdala. J. Neurosci. *10*, 1043–1054.

Lee, Y., López, D.E., Meloni, E.G., and Davis, M. (1996). A primary acoustic startle pathway: obligatory role of cochlear root neurons and the nucleus reticularis pontis caudalis. J. Neurosci. *16*, 3775–3789.

Letzkus, J.J., Wolff, S.B.E., Meyer, E.M.M., Tovote, P., Courtin, J., Herry, C., and Lüthi, A. (2011). A disinhibitory microcircuit for associative fear learning in the auditory cortex. Nature *480*, 331–335.

Li, Y., Xu, J., Liu, Y., Zhu, J., Liu, N., Zeng, W., Huang, N., Rasch, M.J., Jiang, H., Gu, X., et al. (2017). A distinct entorhinal cortex to hippocampal CA1 direct circuit for olfactory associative learning. Nat. Neurosci. *20*, 559–570.

Liang, F., Xiong, X.R., Zingg, B., Ji, X.Y., Zhang, L.I., and Tao, H.W. (2015). Sensory cortical control of a visually induced arrest behavior via corticotectal projections. Neuron *86*, 755–767.

Lingenhöhl, K., and Friauf, E. (1994). Giant neurons in the rat reticular formation: a sensorimotor interface in the elementary acoustic startle circuit? J. Neurosci. *14*, 1176–1194.

Liu, B.H., Li, Y.T., Ma, W.P., Pan, C.J., Zhang, L.I., and Tao, H.W. (2011). Broad inhibition sharpens orientation selectivity by expanding input dynamic range in mouse simple cells. Neuron *71*, 542–554.

Lovett-Barron, M., Kaifosh, P., Kheirbek, M.A., Danielson, N., Zaremba, J.D., Reardon, T.R., Turi, G.F., Hen, R., Zemelman, B.V., and Losonczy, A. (2014). Dendritic inhibition in the hippocampus supports fear learning. Science *343*, 857–863.

Madisen, L., Zwingman, T.A., Sunkin, S.M., Oh, S.W., Zariwala, H.A., Gu, H., Ng, L.L., Palmiter, R.D., Hawrylycz, M.J., Jones, A.R., et al. (2010). A robust and high-throughput Cre reporting and characterization system for the whole mouse brain. Nat. Neurosci. *13*, 133–140.

Miller, C.L., and Freedman, R. (1993). Medial septal neuron activity in relation to an auditory sensory gating paradigm. Neuroscience *55*, 373–380.

Moxon, K.A., Gerhardt, G.A., Bickford, P.C., Austin, K., Rose, G.M., Woodward, D.J., and Adler, L.E. (1999). Multiple single units and population responses during inhibitory gating of hippocampal auditory response in freely-moving rats. Brain Res. *825*, 75–85.

Oh, S.W., Harris, J.A., Ng, L., Winslow, B., Cain, N., Mihalas, S., Wang, Q., Lau, C., Kuan, L., Henry, A.M., et al. (2014). A mesoscale connectome of the mouse brain. Nature *508*, 207–214.

Pitkänen, A., Pikkarainen, M., Nurminen, N., and Ylinen, A. (2000). Reciprocal connections between the amygdala and the hippocampal formation, perirhinal cortex, and postrhinal cortex in rat. A review. Ann. N Y Acad. Sci. *911*, 369–391.

Robinson, J., Manseau, F., Ducharme, G., Amilhon, B., Vigneault, E., El Mestikawy, S., and Williams, S. (2016). Optogenetic activation of septal glutamatergic neurons drive hippocampal theta rhythms. J. Neurosci. *36*, 3016–3023.

Romand, E. (1997). The Central Auditory System (Oxford).

Romanski, L.M., and LeDoux, J.E. (1992). Equipotentiality of thalamo-amygdala and thalamo-cortico-amygdala circuits in auditory fear conditioning. J. Neurosci. *12*, 4501–4509.

Rummell, B.P., Klee, J.L., and Sigurdsson, T. (2016). Attenuation of responses to self-generated sounds in auditory cortical neurons. J. Neurosci. *36*, 12010–12026.

Saunders, A., Granger, A.J., and Sabatini, B.L. (2015). Corelease of acetylcholine and GABA from cholinergic forebrain neurons. eLife *4*, 2015.

Sparta, D.R., Smithuis, J., Stamatakis, A.M., Jennings, J.H., Kantak, P.A., Ung, R.L., and Stuber, G.D. (2014). Inhibition of projections from the basolateral amygdala to the entorhinal cortex disrupts the acquisition of contextual fear. Front. Behav. Neurosci. *8*, 129.

Sun, Y.J., Wu, G.K., Liu, B.H., Li, P., Zhou, M., Xiao, Z., Tao, H.W., and Zhang, L.I. (2010). Fine-tuning of pre-balanced excitation and inhibition during auditory cortical development. Nature *465*, 927–931.

Tao, C., Zhang, G., Zhou, C., Wang, L., Yan, S., Tao, H.W., Zhang, L.I., Zhou, Y., and Xiong, Y. (2017). Diversity in Excitation-Inhibition Mismatch Underlies Local Functional Heterogeneity in the Rat Auditory Cortex. Cell Rep. *19*, 521–531.

Tervo, D.G.R., Hwang, B.Y., Viswanathan, S., Gaj, T., Lavzin, M., Ritola, K.D., Lindo, S., Michael, S., Kuleshova, E., Ojala, D., et al. (2016). A designer AAV variant permits efficient retrograde access to projection neurons. Neuron *92*, 372–382.

van Strien, N.M., Cappaert, N.L.M., and Witter, M.P. (2009). The anatomy of memory: an interactive overview of the parahippocampal-hippocampal network. Nat. Rev. Neurosci. *10*, 272–282.

Vinogradov, O.S. (1975). Functional organization of the limbic system in the process of registration of information: facts and hypotheses. In The Hippocampus, R.L. Issacson and K.H. Pribram, eds. (Springer).

Wan, H., Warburton, E.C., Kuśmierek, P., Aggleton, J.P., Kowalska, D.M., and Brown, M.W. (2001). Fos imaging reveals differential neuronal activation of areas of rat temporal cortex by novel and familiar sounds. Eur. J. Neurosci. *14*, 118–124.

Webster, D.B., Popper, A.N., and Fay, R.R. (1992). The Mammalian Auditory Pathway: Neuroanatomy (Springer-Verlag).

Wickersham, I.R., Finke, S., Conzelmann, K.K., and Callaway, E.M. (2007). Retrograde neuronal tracing with a deletion-mutant rabies virus. Nat. Methods *4*, 47–49.

Winer, J.A. (1992). The functional architecture of the medial geniculate body and the primary auditory cortex. In The Mammalian Auditory Pathway:

Neuroanatomy, D.B. Webster, A.N. Popper, and R.R. Fay, eds. (Springer-Verlag), pp. 222–409.

Wolff, S.B.E., Gründemann, J., Tovote, P., Krabbe, S., Jacobson, G.A., Müller, C., Herry, C., Ehrlich, I., Friedrich, R.W., Letzkus, J.J., and Lüthi, A. (2014). Amygdala interneuron subtypes control fear learning through disinhibition. Nature *509*, 453–458.

Xiong, X.R., Liang, F., Li, H., Mesik, L., Zhang, K.K., Polley, D.B., Tao, H.W., Xiao, Z., and Zhang, L.I. (2013). Interaural level difference-dependent gain control and synaptic scaling underlying binaural computation. Neuron *79*, 738–753.

Xiong, X.R., Liang, F., Zingg, B., Ji, X.Y., Ibrahim, L.A., Tao, H.W., and Zhang, L.I. (2015). Auditory cortex controls sound-driven innate defense behaviour through corticofugal projections to inferior colliculus. Nat. Commun. *6*, 7224.

Xu, M., Chung, S., Zhang, S., Zhong, P., Ma, C., Chang, W.C., Weissbourd, B., Sakai, N., Luo, L., Nishino, S., and Dan, Y. (2015). Basal forebrain circuit for sleep-wake control. Nat. Neurosci. *18*, 1641–1647.

Yao, J.D., Bremen, P., and Middlebrooks, J.C. (2015). Transformation of spatial sensitivity along the ascending auditory pathway. J. Neurophysiol. *113*, 3098–3111.

Yeomans, J.S., Li, L., Scott, B.W., and Frankland, P.W. (2002). Tactile, acoustic and vestibular systems sum to elicit the startle reflex. Neurosci. Biobehav. Rev. *26*, 1–11.

Zhang, L.I., Zhou, Y., and Tao, H.W. (2011). Perspectives on: information and coding in mammalian sensory physiology: inhibitory synaptic mechanisms underlying functional diversity in auditory cortex. J. Gen. Physiol. *138*, 311–320.

Zhou, M., Tao, H.W., and Zhang, L.I. (2012). Generation of intensity selectivity by differential synaptic tuning: fast-saturating excitation but slow-saturating inhibition. J. Neurosci. *32*, 18068–18078.

Zhou, M., Liang, F., Xiong, X.R., Li, L., Li, H., Xiao, Z., Tao, H.W., and Zhang, L.I. (2014). Scaling down of balanced excitation and inhibition by active behavioral states in auditory cortex. Nat. Neurosci. *17*, 841–850.

Zhou, M., Li, Y.T., Yuan, W., Tao, H.W., and Zhang, L.I. (2015). Synaptic mechanisms for generating temporal diversity of auditory representation in the dorsal cochlear nucleus. J. Neurophysiol. *113*, 1358–1368.

Zingg, B., Hintiryan, H., Gou, L., Song, M.Y., Bay, M., Bienkowski, M.S., Foster, N.N., Yamashita, S., Bowman, I., Toga, A.W., and Dong, H.W. (2014). Neural networks of the mouse neocortex. Cell *156*, 1096–1111.

Zingg, B., Chou, X.L., Zhang, Z.G., Mesik, L., Liang, F., Tao, H.W., and Zhang, L.I. (2017). AAV-mediated anterograde transsynaptic tagging: mapping corticocollicular input-defined neural pathways for defense behaviors. Neuron *93*, 33–47.

STAR★METHODS

KEY RESOURCES TABLE

REAGENT or RESOURCE	SOURCE	IDENTIFIER
Antibodies		
Fluorescent Nissl Stain	Invitrogen	N21483
Bacterial and Virus Strains		
AAV9.EF1α.DIO.hChR2(H134R)-EYFP.WPRE.hGH	UPenn vector core	Addgene 20298
pAAV-Syn-GFP	Upenn vector core	Addgene 58867
AAVretro-GFP	Tervo et al., 2016	N/A
ΔG-rabies-GFP	Salk Institute	N/A
Chemicals, Peptides, and Recombinant Proteins		
Kwik-Cast Sealant	WPI	KWIK-CAST
DiI	Invitrogen	D282
lidocaine	Alfa Aesar	T06C018
paraformaldehyde	Alfa Aesar	10194340
NaCl	OmniPur	UI27FZEMS
KCl	Mallinckrodt	7447-40-7
NaHCO$_3$	EMD Chemicals	48204847
MgCl$_2$	J.T. Baker	7791-18-6
CaCl$_2$	EMD Chemicals	41046444
glucose	Sigma	SLBC6575V
sucrose	Millipore	D00168514
Agarose	OmniPur	3332C511
Muscimol, >98%; Tocris; 10 mg	Fisher Scientific	28910
Experimental Models: Organisms/Strains		
Mouse: C57BL/6J	Jackson Lab	Stock No: 000664; RRID: IMSR_JAX:000664
Mouse: Ai14	Jackson Lab	RRID: IMSR_JAX:007914
Mouse: vGlut2-IRES-Cre mice	Jackson Lab	RRID: IMSR_JAX: 016963
Software and Algorithms		
Data acquisition with Labview	Labview	http://www.ni.com; RRID: SCR_014325
Custom-written MATLAB code for analysis	MATLAB	http://www.mathworks.com/; RRID: SCR_001622
Allen Reference Atlas	Dong, 2007	http://www.brain-map.org; RRID: SCR_006491
Mclust	A.D. Redish	http://redishlab.neuroscience.umn.edu/MClust/MClust.html
Offline sorter	Plexon	https://plexon.com
Prism	GraphPad	https://www.graphpad.com/scientific-software/prism/; RRID: SCR_002798
Fiji	NIH	https://fiji.sc/; RRID: SCR_002285
Other		
Free Field Speaker	Vifa XT25G30-04 1" Dual Ring Tweeter	N/A
Sound-Attenuation Booth	Gretch-Ken Industries	N/A
NI board for sound generation	National Instrument	PCI-6731

CONTACT FOR REAGENT AND RESOURCE SHARING

Futher information and requests for resources and reagents should be directed to and will be fulfilled by the Lead Contact, Li I. Zhang (liizhang@usc.edu).

EXPERIMENTAL MODELS AND SUBJECT DETAILS

Experiments were performed in the Zilkha Neurogenetic Institute at the University of Southern California (USC), and experimental procedures in this study were approved by the Animal Care and Use Committee of USC. Male and female C57BL/6J, Ai14 (Cre-dependent tdTomato reporter) mice (Jackson Laboratories, RRID: IMSR_JAX:007914) and vGlut2-IRES-Cre mice (Jackson Laboratories, RRID: IMSR_JAX: 016963) aged 2–3 months were used in this study. Mice were housed with 12-hr light/dark cycles. All recordings and behavioral tests were conducted in the dark cycle.

METHOD DETAILS

Head-fixed animal preparation

Three days before the experiment, the mouse was anesthetized with isoflurane (1.5% by volume), and a screw for head fixation was mounted on top of the skull with dental cement. The head screw was clamped into a metal post to fix the head. The animal was trained to run freely on a flat plate rotating smoothly around its center. One day before electrophysiological recordings, the mouse was anesthetized with isoflurane, and a craniotomy was performed over the intended recording region and then sealed with silicone adhesive (Kwik-Cast Sealant, WPI) until the recording experiments.

In vivo electrophysiological recordings in awake animals

The following recordings and tests were all performed in a sound-attenuation booth (Acoustic Systems). Individual recording sessions lasted for no more than 2 hr. The animal was given drops of 5% sucrose through a tube during recording break. Loose-patch and single-unit extracellular recordings in EC were performed according to previous procedures (Liang et al., 2015; Tao et al., 2017), with a patch pipette filled with an artificial cerebral spinal fluid (ACSF; 126 mM NaCl, 2.5 mM KCl, 1.25 mM Na_2PO_4, 26 mM $NaHCO_3$, 1 mM $MgCl_2$, 2 mM $CaCl_2$ and 10 mM glucose). Axopatch 200B amplifier (Molecular Devices) was used to record signals. A loose seal (0.1–0.5 GΩ) was made on the cell body, allowing spikes only from the patched cell to be recorded in voltage-clamp mode. Signals were filtered with a 300–3,000 Hz band-pass filter. With large pipette openings (resistance < 6 MΩ), no cortical fast-spiking neurons were ever recorded, suggesting that these recording parameters imposed a strong sampling bias toward excitatory neurons, which have larger cell bodies and more extensive dendritic fields than most inhibitory neurons. This bias has also been shown in our previous studies (Ibrahim et al., 2016; Liang et al., 2015; Liu et al., 2011). Single-unit recordings in the MS, PCG, and PRN were performed using a tungsten electrode (0.5 MΩ impedance, WPI). Data were acquired and digitized at 30 kHz sampling rate (Plexon). Coordinates for recording were based on the Allen Reference Atlas (Dong, 2007). Some electrodes were coated with DiI (Invitrogen) for the reconstruction of electrode track (Tao et al., 2017).

Recording in the AC

Auditory cortical regions were pre-mapped with extracellular recordings. The primary auditory cortex was identified by its tonotopic representation of characteristic frequencies in a caudal-to-rostral (low to high frequency) gradient, relatively sharp spike FRAs and short response onset latencies, as we previously described (Sun et al., 2010; Zhou et al., 2014; Tao et al., 2017).

Recording in the MGBv

We mapped the auditory thalamus by extracellular recordings with a parylene-coated tungsten electrode (2 MΩ, FHC). Single units were sorted. Mapping was performed in a three-dimensional manner by systematically varying the depth and the x–y coordinates of the electrode that penetrated the primary auditory cortical surface with an approximately right angle. We distinguished the MGBv (~2.4–2.6 mm below the auditory cortical surface) from other auditory thalamic divisions based on its tonotopic frequency representation, relatively sharp spike FRAs and short onset latencies (Xiong et al., 2015).

Recording in the IC

The IC area was mapped by extracellular recordings with a tungsten electrode. Single units were sorted. The ICC region was identified based on short response latencies (6–8 ms for noise responses), sharply tuned FRAs as well as a dorsal-to-ventral gradient of characteristic frequencies (from low to high), as described in our previous study (Xiong et al., 2013).

Recording in the CN

We mapped the tonotopy of the dorsal part of CN (DCN) with extracellular recordings, which demonstrated a low-high frequency gradient along the lateral-medial axis, as described in our previous study (Zhou et al., 2012; Zhou et al., 2015).

Recording in the ECI

The head of the animal was laterally rotated at 45°. A 1x1 mm^2 craniotomy window was performed over the juncture of temporal, occipital, and interparietal bone (3.75 mm lateral to midline, 4.6 mm posterior to bregma). The electrode was penetrated orthogonal to the cortical surface and below the caudal rhinal vein (~1.75 mm below the pia).

Recording in the ECm
Craniotomy was performed over the ECm (3.5 mm lateral to midline, 4.9 mm posterior to bregma). During recording sessions, the animal head was anteriorly rotated at 7° and electrode was vertically penetrated to a depth of ∼3.5 mm below the pia.

Recording in the MS
Craniotomy was performed over the MS (1 mm lateral to midline, 0.8 mm anterior to bregma). The animal head was laterally rotated at 13°. The electrode was penetrated to a depth of 4–5 mm below pia and recording position was reconstructed after recording.

Recording in the PCG and PRN
Craniotomy was performed over the PCG and PRN (0.5 mm lateral to midline, 5.5mm posterior to bregma). The electrode was penetrated to a depth of 3–4 mm below the pia for PCG and 4.5–5.5 mm below the pia for PRN. Recoding position was confirmed after the reconstruction of the electrode track.

Sound stimulation
A calibrated open field speaker (Vifa XT25G30-04 1" Dual Ring Tweeter) was used for sound delivery. Its position was adjusted according to that of the ear, such that the speaker was 10 cm away from and facing the left ear (contralateral to the recorded brain regions listed above except CN), with the ear canal aligned with the axis of the speaker. Software for sound stimulation and data acquisition was custom developed with LabVIEW (National Instruments, Austin, TX), and PCI-6731 NI board (16-bits output, and 1MHz sampling rate) was used for sound generation. The experimental sequence was the same for each recorded cell: testing of response to 80 dB SPL white noise (20-50 trials, with 5 s inter-stimulus interval), followed by FRA mapping (at least 3 trials) and then by testing of rate-intensity function (20 trials). For FRA mapping, pure tones (2-32 kHz at 0.1-octave intervals, 50 ms duration, 3 ms ramp) at eight, 10 dB-spaced sound intensities (10–80 dB SPL) were delivered in a pseudo-random sequence. The time interval and intensity difference between two sequential tones were set at 0.5 s and no more than 30 dB SPL, respectively, to ensure minimal interactions between tone responses. Characteristic frequency (CF), the frequency at which the neuron responded to tones with the minimum intensity, was determined online. For testing rate-intensity function, broadband white noise (1–64 kHz) at twelve intensities (0–110 dB SPL spaced at 10 dB) were delivered in a pseudo-random sequence (intensity difference between sequential stimuli > 30 dB), with the inter-stimulus interval set as 5 s.

Viral injection
Stereotaxic injection of the virus was carried out as we previously described (Xiong et al., 2015; Zingg et al., 2017). Coordinates for injections followed those for recording. Mice were anesthetized with 1.5% isoflurane. A small cut was made on the skin covering the ECl, ECm, MS, PCG, and PRN and the muscles were removed. One ∼0.2x0.2 mm^2 craniotomy window was made for each region as described in above recording experiments. The following adeno-associated viruses (AAVs, encoding ChR2, or GFP or Cre) or rabies virus (encoding GFP) (Wickersham et al., 2007) were used depending on the purpose of experiments and strain of mice: AAV9.EF1α.DIO.hChR2(H134R)-EYFP.WPRE.hGH (UPenn vector core, Addgene 20298), pAAV-Syn-GFP (Upenn vector core, Addgene 58867), AAVretro-Cre (Tervo et al., 2016), ΔG-rabies-GFP(Salk Institute). A beveled glass micropipette (tip opening diameter: ∼20–30 μm) was used to deliver the virus, and the glass micropipette was attached to a microsyringe pump (World Precision Instruments). For each injection, 50 nL of the viral solution was injected at a rate of 15 nL min^{-1}. Right after the injection, the pipette was allowed to rest for 4 min before withdrawal. The scalp was then sutured. Following the surgery, 0.1 mg kg^{-1} buprenorphine was injected subcutaneously before returning the animals back to their home cages. Mice were allowed to recover for at least 3 weeks.

Optogenetic activation
To activate MS glutamatergic axon terminals in EC, an optic fiber (200 μm, Thorlabs) connecting to a blue LED source (473 nm, Thorlabs) was positioned close to the surface of ECl. The tip of the optic fiber was covered by agar stained with black pigments to prevent light leakage. To ensure the specificity of the optogenetic stimulation, no ChR2-expressing fibers and structures other than the targeted structure should be present in the light pathway within 800 μm from the end of the optic fiber. The axis of the light pathway was the same as the central axis of the optic fiber, and the illumination angle was determined by the fiber's NA value. This rule applied to all of our experiments. After each experiment, the brain was sectioned and imaged under a fluorescence microscope to confirm the expression of ChR2-EYFP.

Silencing of brain structures
Lidocaine, a blocker of the voltage-gated Na$^+$ channel (2%, dissolved in ACSF containing biotinylated dextran amines, BDA), or fluorescent muscimol BODIPY (0.7 mM in ACSF with 5% DMSO) was used to silence a targeted brain region. The drug was applied via implanted cannulas (OD, 300 μm; ID, 140 μm). The silencing efficiency was evaluated for each experiment by comparing the evoked spike responses before and after the perfusion of the drug (Figure S4). To silence the AC (lidocaine, volume, 150 nL per hemisphere), the cannula was inserted to a depth of 400 μm below the cortical surface centered on A1. For MS silencing (lidocaine, volume, 150 nL), the cannula was inserted to a depth of 4250 μm below the surface. For PCG silencing (muscimol, 100 nL per hemisphere), the cannula was inserted to a depth of 2300 μm below the surface. The spread of lidocaine was estimated by the fluorescent imaging of BDA. Two hours after injection, the animals were transcardially perfused with 4%

paraformaldehyde in phosphate-buffered saline. Coronal brain sections (100 μm) were made with a vibratome (Leica Microsystems) and imaged under a confocal microscope (Olympus). For electrolytic lesion, a parylene-coated tungsten electrode (tip diameter, 45 μm) was implanted to target MS, or AC using the same methods as described above. A direct current of 1mA from a current source (Keithley Instruments) was applied for 10 s.

Fear conditioning

Mice underwent auditory fear conditioning in custom-made behavioral boxes in a sound-attenuation booth (Gretch-Ken Industries). The training box was a hard paper box with metal wires on the bottom, and the testing box was an acrylic box with bedding materials. The conditioning chamber and the test box were cleaned with 70% ethanol before and after each session. The bedding material in the test box was replaced before each test session. On the first day, after 10 min habituation to the conditioning chamber, animals were exposed to white noise (80 dB SPL, duration = 20 s) for 5 times to measure the basal level response. On the second day (conditioning), the animals were exposed to the 20 s noise co-terminated with a 0.75-mA foot shock (5Hz for 1 s with the duration of each pulse = 100 ms) for 5 times. On the third day, mice were placed in a different context (test box) and given 5 noise presentations in the absence of foot shocks. Inter-trial interval for noise presentation was randomly chosen from a range of 120 s to 240 s with the mean of 180 s. All the processes were video recorded, and a blind procedure was implemented for behavioral analysis. The fear response was scored as the percentage of time freezing during the 20 s presentation of noise alone. The freezing was scored when no movement (except for respiratory movements) was detected for at least 1 s, and the total freezing time during a sound presentation was counted based on the video analysis.

Test of the Preyer's reflex

Mice underwent tests of the Preyer's reflex in a custom-made behavioral box placed in a sound-attenuation booth (Gretch-Ken Industries). We conducted testing in the dark. The movement of the animal was monitored using a high speed (240 fps) camera. The animal was exposed to 80 dB SPL, 200-ms white noise or tones (7.5kHz) for 10 times with a randomly chosen inter-stimulus interval (3-5 min. A quick movement of pinna within 50 ms after the onset of sound stimulation was considered as a successful trial.

QUANTIFICATION AND STATISTICAL ANALYSIS

Data processing

FRAs were reconstructed according to the array sequence. CF was defined as the frequency that evoked reliable spike responses at the lowest intensity level. Response onset latency was determined from the PSTH by the time point at which spiking activity exceeded the average baseline firing rate (measured during the 100-ms time window before the stimulus onset) by 3 standard deviations of baseline fluctuations. Offline spike sorting (Mclust, written by A.D. Redish, http://redishlab.neuroscience.umn.edu/MClust/MClust.html; Offline sorter, Plexon) was applied to isolate single units. The signal-to-noise ratio in our recordings was usually > 10dB. Analysis performers were blind to the allocation of the experiments. All data were first pooled together without categorizing the neurons according to their recording sites, and randomized batch processing was then performed.

The Z-score was calculated as the evoked firing rate (calculated within a 50-ms window after the stimulus onset) divided by the standard deviation of the baseline firing rate (calculated within a 100-ms window before the stimulus onset).

Statistics

Shapiro–Wilk test was first applied to examine whether samples had a normal distribution. Leven's test was used to test the equality of variances. In the case of a normal distribution, t test, paired t test or analysis of variance test was applied. In the case of unequal variance, t test with equal variance not assumed was used. In the case of homogeneous variance, one-way ANOVA with Tukey post hoc test was used; in the case of inhomogeneous variance, one-way ANOVA with Tamhane post hoc test was applied. Data were presented as mean ± SD if not otherwise specified.